Time-Aware Topological Graph Convolutional Networks for Wildfire Prediction

••

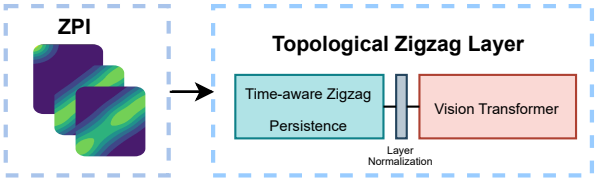

Figure 1: Topological Zigzag Layer

Abstract

1 Firecast Zigzag Graph Convolutional Network (FZ−GCN)

We address wildfire risk prediction as a binary classification problem. Given spatio-temporal information $\mathbf{X}_t$ we want to classify if a pixel-of-interest (POI) will be on fire on the next time $(t+1)$. This problem is popularly known as pixel-wise classification.

Our proposal Firecast Zigzag Graph Convolutional Network (FZ−GCN) is different from past wildfire prediction methods because of it includes topological features by means of graph modeling. Graph modeling allows it to discover hidden relations and to capture spatio-temporal context. Recently, GCN have been used with spatio-temporal data for different tasks, and showed powerful capabilities [Chen *et al.*, 2022]. Here we propose an architecture that combines information of a topological zigzag layer with a topological Graph Convolutional Layer by means of a Gate Recurrent Unit. This process is detailed in Figure 3, where the sptaio-temporal information is used as input for each layer.

First, it applies a topological zigzag layer (Figure 1) which uses ZPI information. Formaly, it is defined as follows:

$$\mathbf{ZO} = ViT(\mathbf{PI}) \tag{1}$$

where $\mathbf{PI} \in \mathbb{R}^{p \times p}$ and $\mathbf{ZO} \in \mathbb{R}^{2 \times 1}$. Note that depending on the configuration, a zigzag filtration might generate different signatures. For simplicity, in our case we concatenate p-dimensional topological features (0-dimensional and 1-dimensional holes) as different input channels. Then, the zigzag information is passed through a layer normalization, which enables smoother gradients, faster training times, and achieves better generalization [Xu *et al.*, 2019]. Afterthat, a ViT is used to learn the topological patterns that can be found in the ZPI. Note that this ViT version uses multi-head mechanisms attentions, and position embedding that allows it the extraction of ZPI information efficiently [Dosovitskiy *et al.*, 2020]. Second, we include a Graph Convolutional Layer (Figure 2), it first apply node embedding to the input information, which is used to downstream the amount of nodes. Node embedding is an important step in this layer since it allows to capture the topology of the network. In this problem each pixel is modeled as a node, therefore the efficiency of the network might be compromised by the size of an image, however by applying node embedding the resolution of the input image is not longer a problem. Then, this layer includes spatial and temporal graph convolution, respectively. While the former is to capture spatial correlation between nodes, the later is to capture temporal correlation between features in differen time slices. We adopted Equation (**??**) in our arquitecture to apply spatial convolutions, where $\mathbf{W}_1$ and $\mathbf{W}_2$ are trainable weights of the network, $\mathbf{P}_1$ is computed with a power series of the adjacency matrix $\mathbf{A}$. The output of this spatial convolution is multiplied by a hidden matrix $\mathbf{W}_3$ as follows:

$$\mathbf{S} = \mathbf{Z}\mathbf{W}_3| \tag{2}$$

where $\mathbf{W}_3 \in \mathbb{R}^{M \times H/2}$ and $\mathbf{S} \in \mathbb{R}^{N \times H/2}$.

In addition to the spatial domain, we apply a convolution to all the time slices of the graph as follows:

$$\mathbf{L} = \mathbf{W}_4\mathbf{X}\mathbf{W}_5 \tag{3}$$

where $\mathbf{W}_4 \in \mathbb{R}^{T \times 1}$ is a vector of learnable weights, $\mathbf{W}_5 \in \mathbb{R}^{C_{in} \times H/2}$ is a hidden matrix, and $\mathbf{L} \in \mathbb{R}^{N \times H/2}$ is the output of the temporal convolution. On the last step of the graph convolutional layer are concatenated the outputs of the spatial convolution ($\mathbf{Z}$) and temporal convolution ($\mathbf{L}$) as $\mathbf{Q} = Dense(COMBINE(\mathbf{Z}, \mathbf{L}))$, where $\mathbf{Q} \in \mathbb{R}^{2 \times 1}$. The output of combining both layers is downsized by a dense layer. Note that in several parts of the network is included a layer normalization layer which enables smoother gradients, faster training times, and achieves better generalization [Xu *et al.*, 2019]. Finally, information of both layers $\mathbf{ZO}$ and $\mathbf{Q}$ are added and passed to the binary cross entropy loss function.

2 Experiments

We illustrate the proposed FZ−GCN model in application to forecasting wildfire occurences in Eastern Mediterranean and

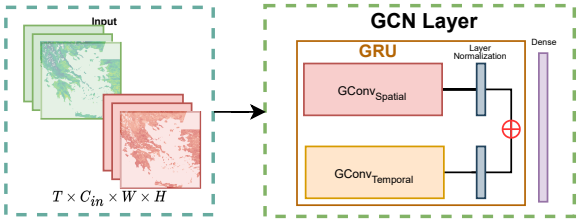

Figure 2: Graph Convolutional Network Layer

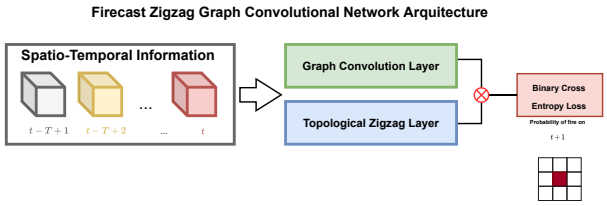

Figure 3: Architecture of FZ−GCN. Spatio-temporal information is given as input to GCN layer and Topological Zigzaf Layer, then the output of each layer is combined and processed by the binary cross entropy loss, which represents the probability of fire on a pixel-of-interest.

the African continent at various resolutions. We also conduct an ablation study to assess individual contributions of the FZ−GCN components. Additional experiments are available in Appendix A.

2.1 Datasets

We consider two regions: Eastern Mediterranean and surrounding areas (defined in a lower resolution) and the African continent (defined in a higher resolution).

Eastern Mediterranean We consider the dataset proposed in [Kondylatos *et al.*, 2022], which consists of 1 km × 1 km × 1 day resolution. The region of interest of this dataset is centered around Greece covering a total area of $1,253$ km × 983 km. Note that, we consider the following 25 variables as predictors and can be grouped as follows:

- *Daily wheater data* from ERA-5 [Muñoz-Sabater *et al.*, 2021]: Land of maximum 2m temperature, maximum wind speed, minimum relative humidity, total precipitation, maximum 2m dew point temperature, and maximum surface pressure.
- *Saltellite variables* from MODIS: Normalized Difference Vegetation Index (NDVI), Day and Night Land Surface Temperature.
- *Soil* from the European Drought Observatory [Cammalleri *et al.*, 2017]: *Soil moisture index*.
- *Geographic and Demographic* from Worldpop [Tatem, 2017] and (ref) Copernicus EU-DEM: Roads distance, waterway distance, yearly population density, elevation and slope.
- Data collection on land from Copernicus Corine Land Cover [Büttner, 2014]

Note that the first ten variables are dynamic and the remaining ones are static. For this dataset the years from 2009 to 2018 are for training set and 2019 for validation set. Regarding testing set, we take into account two sets, one for each year; years 2020 and 2021. All four datasets consists of $40,554$ training ($27,036$ nonfire, $13,518$ fire), $3,900$ validation ($2,600$ nonfire, $1,300$ fire), $3,684$ testing ($2,456$ nonfire, $1,228$ fire) samples for 2020, and $13,221$ testing ($8,814$ nonfire, $4,407$ fire) samples for 2021. To overcome the problem of highly unbalanced classes caused by the scarcely amount of fires, on each run the negatives are randomly sampled two times compared to postives [Huot *et al.*, 2020]. Since our goal is to predict the center pixel and to decrease the risk of sampling negatives that in fact represent fire dangers different to the center pixel, this sampling process selects negatives from days when no fire occurred on the entire patch or region of interest. In this dataset, we used two modalities of samples: temporal and spatio-temporal. The temporal dataset consists of the time series of days $\{t-1, t-2, \ldots, t-10\}$ of the dynamic input observations, which exploits the temporal context. Furthermore, the spatial-temporal dataset consists of 25 km × 25 km × 10 days blocks of the dynamic input observations centered spatially around the given cell. Note that some features are static (e.g. yearly population density) therefore are repeated in time.

African continent We further study the benefits of our proposed method by analyzing its performance accross developing regions in the African continent. In particular, we build a dataset for the Africa continent by taking as source the scientific datacube for seasonal fire forecasting around the globe [Alonso *et al.*, 2022]. This dataset consists of a 0.25 degrees spatial resolution, and 8 days of temporal resolution. Next 7 variables serve as input features in our experiments: total precipitation, sea surface temperature, average temperature at 2 Meters, drought code average, Normalized Difference Vegetation Index (NDVI), population density, and Downwards Surface Solar Radiation (DSSR).

Similarly, this dataset consists of spatio-temporal blocks of 5 km × 5 km × 10 time dimensions, where each time slice is the average along 8 days. Here, the tranining set is taken from years 2009-2017, thus the validation set comes from 2018; whilst for testing we use years 2019 and 2020. All our datasets consists of $9,000$ samples for training (1000 samples per year), and $16,000$ samples for each remaining set.

2.2 Experimental Settings

This experimental validation takes into account two baseline methods widely used for wildfire prediction: LSTM, from [Hochreiter and Schmidhuber, 1997], and ConvLSTM, from [Shi *et al.*, 2015]. Note that both methods are considered as standard for image processing tasks. Our experimentation was carried out on NVIDIA Tesla T4 GPU card with 32GB of memory. LSTM and ConvLSTM were configured as suggested by their authors [Kondylatos *et al.*, 2022]. GCN and FZ−GCN use 1 hidden GCN layer with size 18, node embedding of size 64, and spatial convolution size $K = 2$. Each method was run 10 times on their validation set using differ-

ent seeds, stopping criterion of 30 epochs, batch size equals to 256, and L2-Regularization weight of 0.001.

3 Ablation study

To have compelling insights on the importance of each component within FZ−GCN, we conduct ablation studies on the Eastern Mediterranean dataset, focused on Greece, and present the results in Table 3. In particular, we test FZ−GCN w/o the zigzag learning module, spatial graph convolution, fixed adjacency matrix, and self-adaptive adjacency matrix. Note that the last two elements aim to verify the contribution using a static adjacency matrix, and learning an adjacency matrix, respectively. Results confirms that each component is beneficial for FZ−GCN. Specifically, we can found that, for AUC, the relative gains of FZ−GCN over FZ−GCN w/o Zigzag learning are 1.603% and 0.408% on datasets in Year 2020 and Year 2021; for AUCPR, the relative gains of FZ−GCN over FZ−GCN w/o Zigzag learning are 2.911% and 0.721% on datasets in Year 2020 and Year 2021. Although removing the spatial graph convolutions produces an improvement in terms of precision, this action deteriorates the F1-Score metric and Accuracy. Similarly, removing a fixed adjacency matrix improves the Recall but deteriorates the remaining metrics. These results reveal that inclusion of the zigzag topological layer is needed in order to improve the wildfire prediction and overall performance of the proposed FZ−GCN. Finally, it is relevant to remark that each variant in this ablation study performs better than all base-line methods in terms of F1-Score and Accuracy, which supports the effectiveness of our TDA-based DL model.

4 Lessons Learned and Path to Deployment

5 Conclusion and Future Work

Year 2020	Precision	Recall	F1-Score	Accuracy	AUC	AUCPR
ConvLSTM	0.842 ± 0.032	0.660 ± 0.030	0.739 ± 0.027	84.52% ± 0.015	0.911 ± 0.023	0.857 ± 0.030
LSTM	0.834 ± 0.026	0.696 ± 0.046	0.757 ± 0.023	85.18% ± 0.010	0.923 ± 0.005	0.864 ± 0.008
GCN	0.877 ± 0.014	0.683 ± 0.024	0.768 ± 0.015	86.24% ± 0.007	0.936 ± 0.004	0.893 ± 0.007
FZ-GCN	**0.907** ± 0.016	**0.706** ± 0.025	**0.793** ± 0.012	**87.76%** ± 0.005	**0.951** ± 0.003	**0.919** ± 0.006
Year 2021	**Precision**	**Recall**	**F1-Score**	**Accuracy**	**AUC**	**AUCPR**
ConvLSTM	0.901 ± 0.019	0.905 ± 0.027	0.903 ± 0.015	93.49% ± 0.009	0.978 ± 0.006	0.958 ± 0.012
LSTM	0.891 ± 0.015	0.859 ± 0.039	0.874 ± 0.019	91.77% ± 0.010	0.942 ± 0.003	0.942 ± 0.007
GCN	0.923 ± 0.012	0.905 ± 0.012	0.914 ± 0.009	94.31% ± 0.006	0.981 ± 0.002	0.964 ± 0.005
FZ-GCN	**0.946** ± 0.008	**0.908** ± 0.005	**0.927** ± 0.003	**95.21%** ± 0.002	**0.985** ± 0.000	**0.971** ± 0.002

Table 1: Wildfire risk prediction comparison between different DL methods on test set 2020 and test set 2021. Note that year 2020 represents a typical fire season and year 2021 respresents an extreme one,

	Year 2019				Year 2020			
	Precision	**Recall**	**F1-Score**	**Accuracy**	**Precision**	**Recall**	**F1-Score**	**Accuracy**
ConvLSTM	0.949 ± 0.005	0.984 ± 0.007	0.966 ± 0.004	96.6% ± 0.004	0.966 ± 0.005	0.967 ± 0.006	0.966 ± 0.004	96.6% ± 0.004
GCN	0.965 ± 0.011	**0.994** ± 0.001	0.979 ± 0.005	97.9% ± 0.006	0.972 ± 0.010	0.986 ± 0.003	0.979 ± 0.004	97.9% ± 0.005
FZ-GCN	**0.979** ± 0.006	0.992 ± 0.002	0.986 ± 0.002	**98.5%** ± 0.002	**0.978** ± 0.006	**0.987** ± 0.002	**0.982** ± 0.003	**98.2%** ± 0.003

Table 2: Wildfire risk prediction comparison between spatio-temporal DL methods on test sets 2019 (left side) and 2020 (right side) on the African continent.

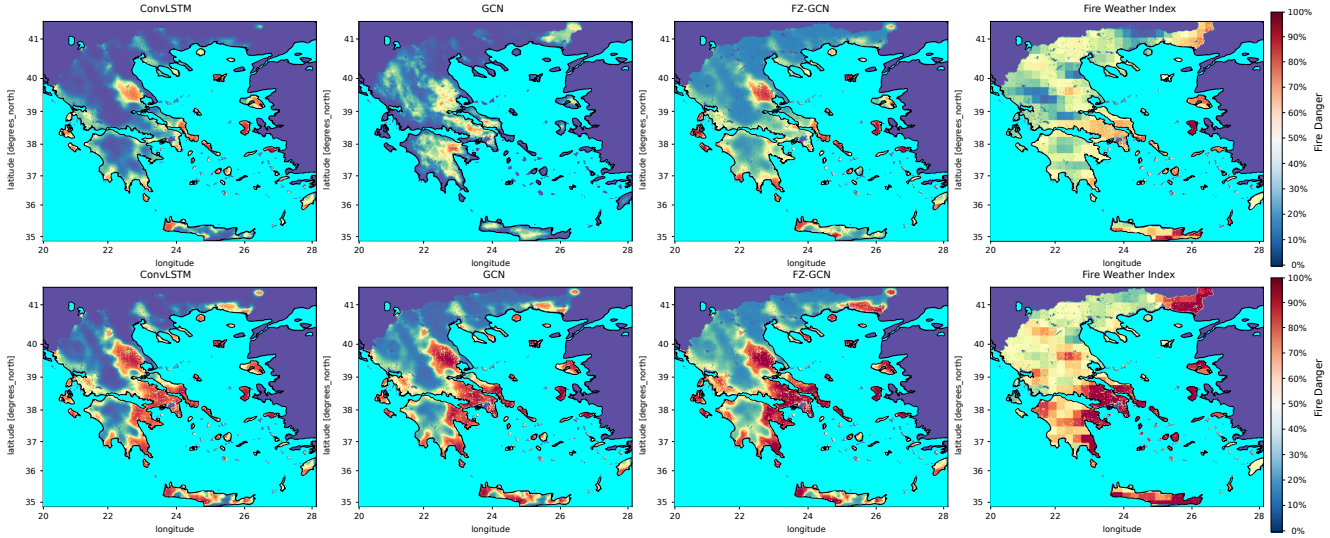

Figure 4: Fire danger for Greece on days 19/07/2020 (top) and 21/07/2020 (bottom). DL methods offers a better resolution than the empirical Fire Weather Index.

Year 2020	Precision	Recall	F1-Score	Accuracy	AUC	AUCPR
FZ-GCN	0.907 ± 0.016	**0.706** ± 0.025	**0.793** ± 0.012	**87.8%** ± 0.005	**0.951** ± 0.003	**0.919** ± 0.006
W/o Zigzag learning	0.877 ± 0.014	0.683 ± 0.024	0.768 ± 0.015	86.2% ± 0.007	0.936 ± 0.004	0.893 ± 0.007
W/o $GCN_{Spatial}$	**0.918** ± 0.014	0.660 ± 0.017	0.768 ± 0.009	86.7% ± 0.004	0.946 ± 0.003	0.909 ± 0.005
W/o Adjacency	0.893 ± 0.007	0.686 ± 0.012	0.776 ± 0.006	86.8% ± 0.003	0.940 ± 0.003	0.900 ± 0.004
W/o Self-Adaptive Adjacency	0.880 ± 0.033	0.701 ± 0.054	0.778 ± 0.020	86.7% ± 0.006	0.942 ± 0.003	0.902 ± 0.006
Year 2021	**Precision**	**Recall**	**F1-Score**	**Accuracy**	**AUC**	**AUCPR**
FZ-GCN	**0.946** ± 0.008	0.908 ± 0.005	**0.927** ± 0.003	**95.2%** ± 0.002	**0.985** ± 0.000	**0.971** ± 0.002
W/o Zigzag learning	0.923 ± 0.012	0.905 ± 0.012	0.914 ± 0.009	94.3% ± 0.006	0.981 ± 0.002	0.964 ± 0.005
W/o $GCN_{Spatial}$	0.944 ± 0.009	0.907 ± 0.005	0.925 ± 0.003	95.1% ± 0.002	0.984 ± 0.001	0.970 ± 0.004
W/o Adjacency	0.933 ± 0.008	**0.911** ± 0.009	0.922 ± 0.003	94.9% ± 0.002	0.983 ± 0.001	0.966 ± 0.005
W/o Self-Adaptive Adjacency	0.944 ± 0.009	0.907 ± 0.005	0.925 ± 0.003	95.1% ± 0.002	0.984 ± 0.001	0.970 ± 0.004

Table 3: Ablation study of the FZ-GCN.

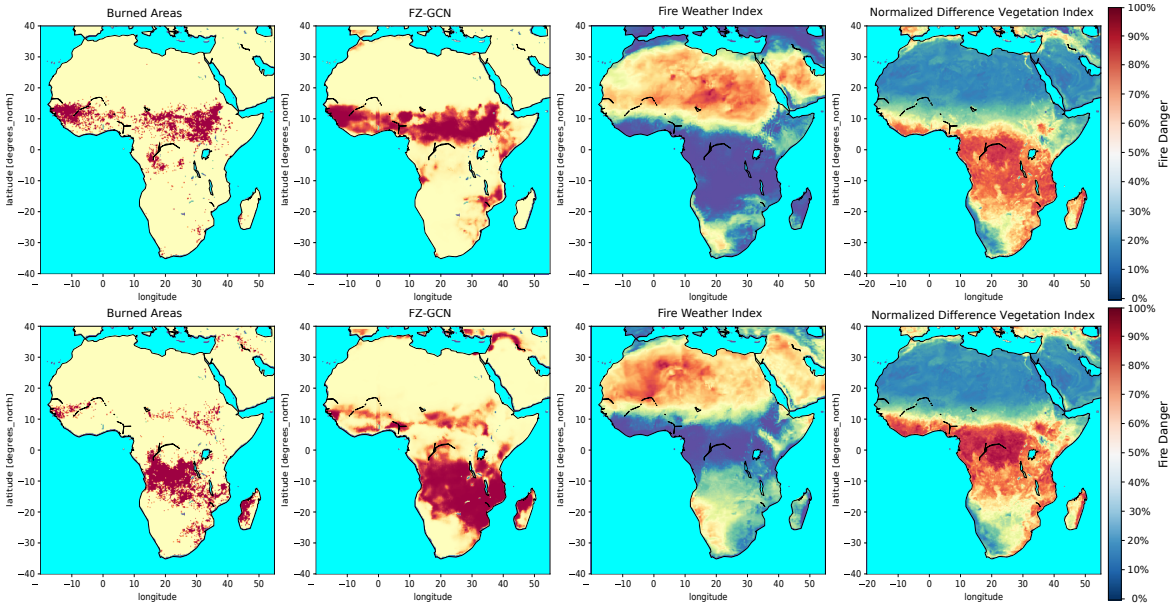

Figure 5: Fire danger for Africa on days 21/03 /2020 (top) and 16/05/2020 (bottom). Each date represents the average of 8 days. Reported are Burned Areas, FZ−GCN, Fire Weather Index, and Normalized Different Vegetation Index, respectively.

References

[Alonso *et al.*, 2022] Lazaro Alonso, Fabian Gans, Ilektra Karasante, Akanksha Ahuja, Ioannis Prapas, Spyros Kondylatos, Ioannis Papoutsis, Eleannna Panagiotou, Dimitrios Mihail, Felix Cremer, Ulrich Weber, and Nuno Carvalhais. SeasFire Cube: A Global Dataset for Seasonal Fire Modeling in the Earth System, September 2022. The creation of this cube has been funded by the European Space Agency (ESA), in the context of ESA Future EO-1 Science for Society Call.

[Büttner, 2014] György Büttner. Corine land cover and land cover change products. *Land use and land cover mapping in Europe: practices & trends*, pages 55–74, 2014.

[Cammalleri *et al.*, 2017] Carmelo Cammalleri, Jürgen V Vogt, Bernard Bisselink, and Ad de Roo. Comparing soil moisture anomalies from multiple independent sources over different regions across the globe. *Hydrology and Earth System Sciences*, 21(12):6329–6343, 2017.

[Chen *et al.*, 2022] Yuzhou Chen, Ignacio Segovia-Dominguez, Baris Coskunuzer, and Yulia Gel. Tamps2gcnets: coupling time-aware multipersistence knowledge representation with spatio-supra graph convolutional networks for time-series forecasting. In *International Conference on Learning Representations*, 2022.

[Dosovitskiy *et al.*, 2020] Alexey Dosovitskiy, Lucas Beyer, Alexander Kolesnikov, Dirk Weissenborn, Xiaohua Zhai, Thomas Unterthiner, Mostafa Dehghani, Matthias Minderer, Georg Heigold, Sylvain Gelly, et al. An image is worth 16x16 words: Transformers for image recognition at scale. *arXiv preprint arXiv:2010.11929*, 2020.

[Hochreiter and Schmidhuber, 1997] Sepp Hochreiter and Jürgen Schmidhuber. Long short-term memory. *Neural computation*, 9(8):1735–1780, 1997.

[Huot *et al.*, 2020] Fantine Huot, R Lily Hu, Matthias Ihme, Qing Wang, John Burge, Tianjian Lu, Jason Hickey, Yi-Fan Chen, and John Anderson. Deep learning models for predicting wildfires from historical remote-sensing data. *arXiv preprint arXiv:2010.07445*, 2020.

[Kondylatos *et al.*, 2022] Spyros Kondylatos, Ioannis Prapas, Michele Ronco, Ioannis Papoutsis, Gustau Camps-Valls, María Piles, Miguel-Ángel Fernández-Torres, and Nuno Carvalhais. Wildfire danger prediction and understanding with deep learning. *Geophysical Research Letters*, 49(17):e2022GL099368, 2022.

[Muñoz-Sabater *et al.*, 2021] Joaquín Muñoz-Sabater, Emanuel Dutra, Anna Agustí-Panareda, Clément Albergel, Gabriele Arduini, Gianpaolo Balsamo, Souhail Boussetta, Margarita Choulga, Shaun Harrigan, Hans Hersbach, et al. Era5-land: A state-of-the-art global reanalysis dataset for land applications. *Earth System Science Data*, 13(9):4349–4383, 2021.

[Shi *et al.*, 2015] Xingjian Shi, Zhourong Chen, Hao Wang, Dit-Yan Yeung, Wai-Kin Wong, and Wang-chun Woo. Convolutional lstm network: A machine learning approach for precipitation nowcasting. *Advances in neural information processing systems*, 28, 2015.

[Tatem, 2017] Andrew J Tatem. Worldpop, open data for spatial demography. *Scientific data*, 4(1):1–4, 2017.

[Xu *et al.*, 2019] Jingjing Xu, Xu Sun, Zhiyuan Zhang, Guangxiang Zhao, and Junyang Lin. Understanding and improving layer normalization. *Advances in Neural Information Processing Systems*, 32, 2019.